

Supplemental information

**DNAJB1-PRKACA fusion neoantigens elicit rare
endogenous T cell responses that potentiate
cell therapy for fibrolamellar carcinoma**

Allison M. Kirk, Jeremy Chase Crawford, Ching-Heng Chou, Cliff Guy, Kirti Pandey, Tanya Kozlik, Ravi K. Shah, Shanzou Chung, Phuong Nguyen, Xiaoyu Zhang, Jin Wang, Matthew Bell, Robert C. Mettelman, E. Kaitlynn Allen, Mikhail V. Pogorelyy, Hyunjin Kim, Anastasia A. Minervina, Walid Awad, Resha Bajracharya, Toni White, Donald Long Jr., Brittney Gordon, Michelle Morrison, Evan S. Glazer, Andrew J. Murphy, Yixing Jiang, Elizabeth A. Fitzpatrick, Mark Yarchoan, Praveen Sethupathy, Nathan P. Croft, Anthony W. Purcell, Sara M. Federico, Elizabeth Stewart, Stephen Gottschalk, Anthony E. Zamora, Christopher DeRenzo, Scott E. Strome, and Paul G. Thomas

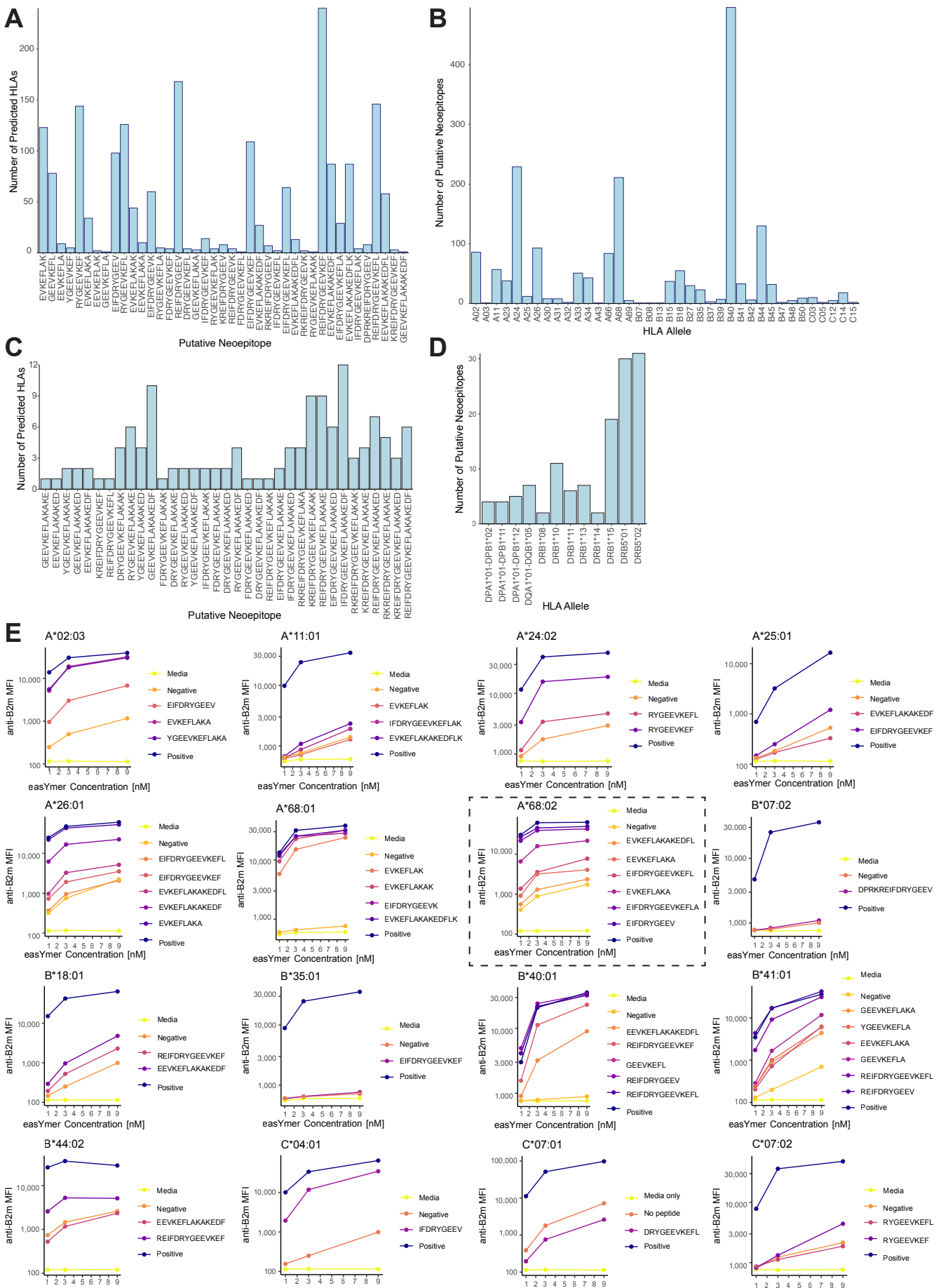
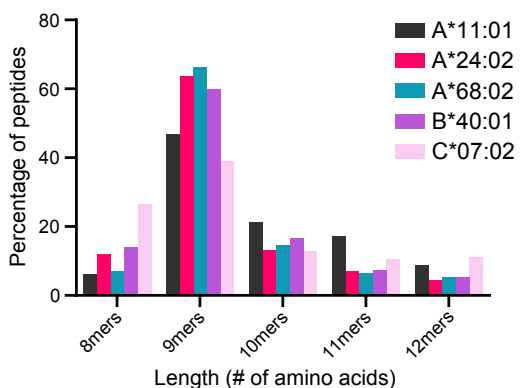


Figure S1. Fusion neoantigen binding to diverse class I HLAs, related to Figure 2. (A) Number of class I HLA alleles predicted to bind given fusion peptides with predicted affinity less than or equal to 500 nM (NetMHCcons1.1 [S1]). (B) Number of fusion peptides predicted to bind to given class I HLA alleles (2-digit resolution) with a predicted affinity of less than or equal to 500 nM (NetMHCcons1.1). (C) Number of class II HLA alleles predicted to bind given fusion peptides with predicted affinity less than or equal to 1000 nM (NetMHCIIPan4.1 [S2]). (D) Number of fusion peptides predicted to bind to given HLA alleles (2-digit resolution) with a predicted affinity of less than or equal to 1000 nM (NetMHCIIPan4.1). (E) Biochemical binding assay results for all 16 class I HLA alleles tested (see Methods). Boxed allele A*68:02 is represented in Figure 2C.

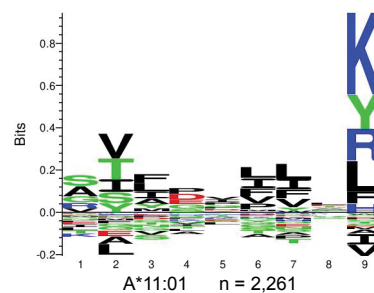
A Total Number of Peptides Eluted

HLA Allele	Number of Peptides
A*11:01	4,842
A*24:02	4,262
A*68:02	3,648
B*40:01	4,555
C*07:02	1,788
Total	19,095

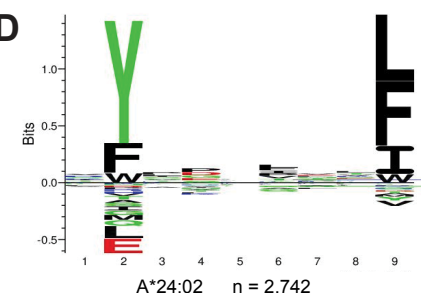
B



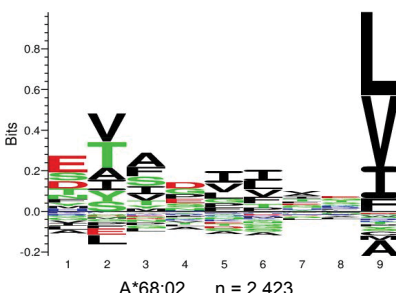
C



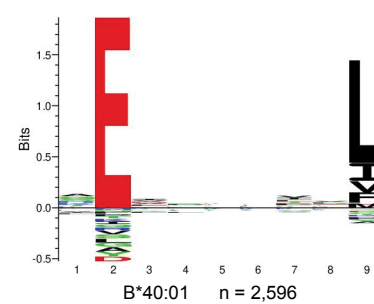
D



E



F



G

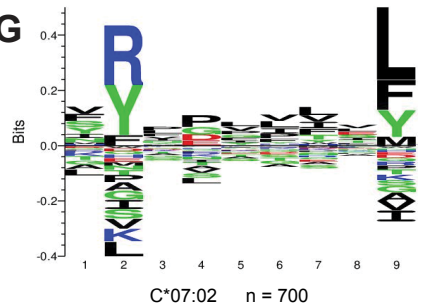


Figure S2. Peptides eluted from HLA K562 cell lines follow canonical peptide length distribution and have canonical binding motifs, related to Figure 2. (A) Total number of HLA class I peptides identified in K562 cell lines expressing class I HLA alleles and the *DNAJB1-PRKAC4* fusion. (B) Length distribution of HLA class I peptides eluted from HLA K562 cell lines. As expected, the majority of peptides identified in each cell line were nonamers followed by longer peptides of 10 and 11mers, except in the case of C*07:02. (C-G) Seq2logo representation of motifs of nonamer peptides identified from A*11:01 (C), A*24:02 (D), A*68:02 (E), B*40:01 (F), and C*07:02 (G), with n representing the number of nonamers identified for each allele.

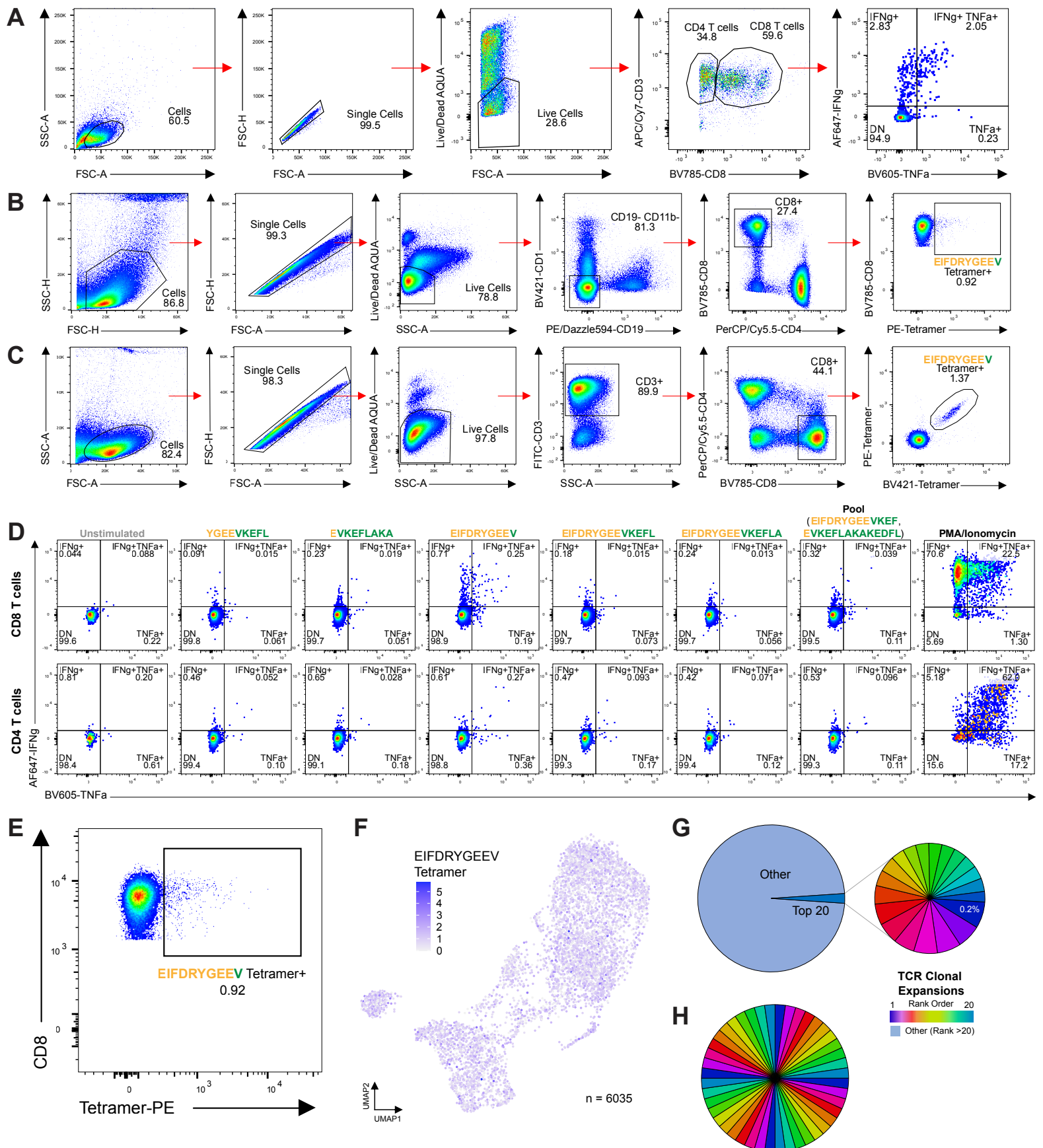


Figure S3. Unexpanded PBMCs from patient FLC-SJ1 contain tetramer-positive T cells, but no clonal expansions, related to Figure 3. (A) Gating strategy for Figure 3B and Figure S3D. (B) Gating strategy for Figure S3E. (C) Gating strategy for Figure 3E. (D) Intracellular cytokine staining for IFN γ and TNF α of patient FLC-SJ1 tumor infiltrating lymphocytes (TILs) stimulated with indicated fusion peptides or control reagents. This panel represents an independent experiment from that shown in Figure 3B. (E) A*68:02-EIFDRYGEEV tetramer staining of unexpanded PBMCs from patient SJ1. Frequency of tetramer-positive cells reflects expected proportion of tetramer-positive cells in 10x data. (F) UMAP plot highlighting barcoded A*68:02-EIFDRYGEEV tetramer labeling among cells captured by 10x single-cell gene expression and paired TCR sequencing. Total number of cells represented by UMAP=6035. (G) Clonal expansions among unexpanded PBMCs from patient SJ1. Expanded pie chart represents the top 20 most frequent clonotypes, the most frequent of which occurred at a frequency of 0.2%. (H) Clonotype frequency among all tetramer-positive clonotypes (n=44) detected in 10x data. No TCR clones were expanded among tetramer-positive cells.

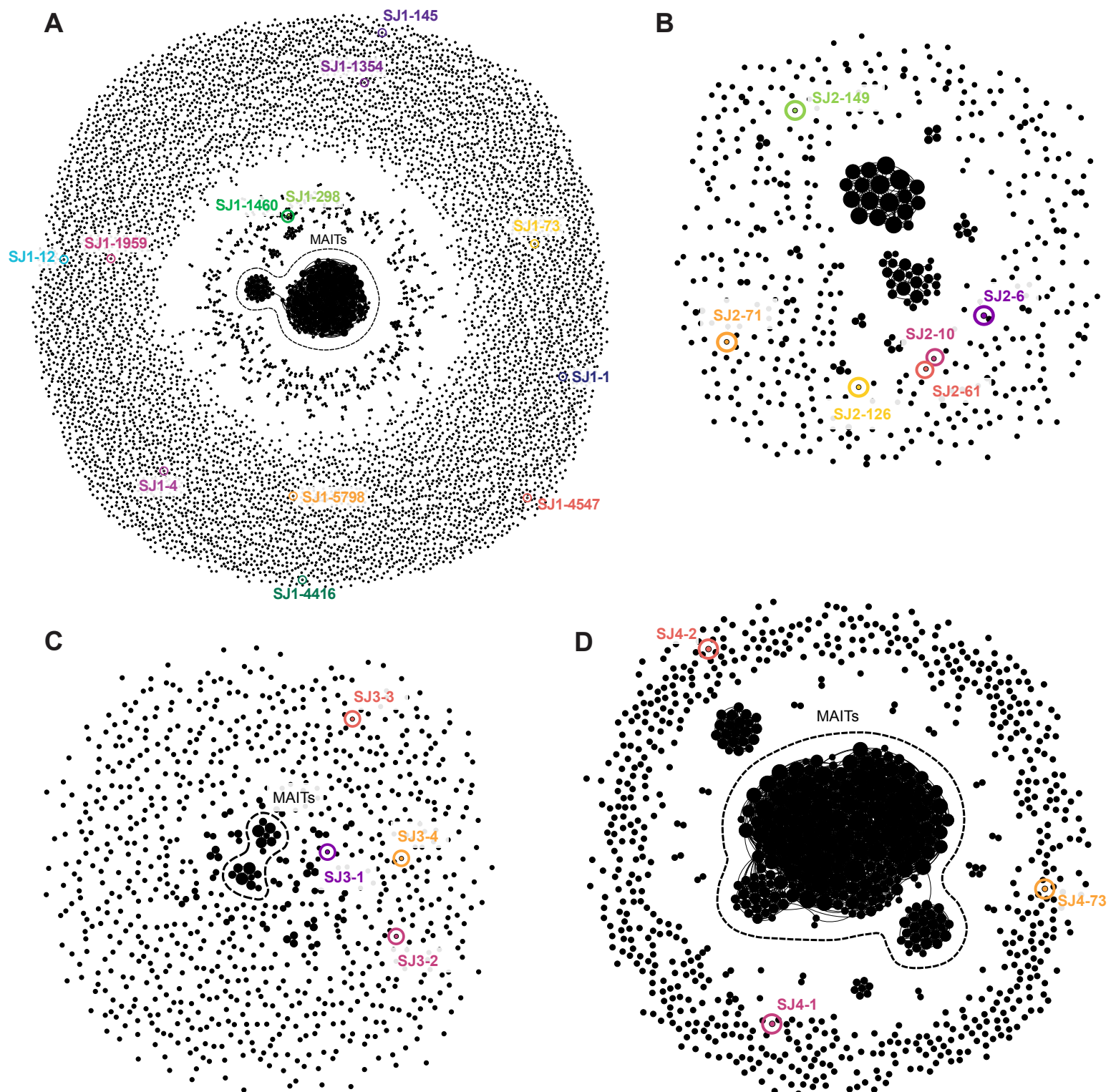


Figure S4. TCRdist mapping of all TCR clones selected for validation, related to Figure 4. (A-D) TCRdist network of unique, paired TCRs from patients FLC-SJ1 (A), SJ2 (B), SJ3 (C), and SJ4 (D). Each node represents a unique TCR clonotype, and two nodes are connected by an edge if their TCRdist<100; node size corresponds to the node degree (number of neighbors). Large central clusters in A, C, and D represent mucosal-associated invariant T (MAIT) cells. The location of each TCR selected for validation, as shown in Figure 4B and C, is indicated.

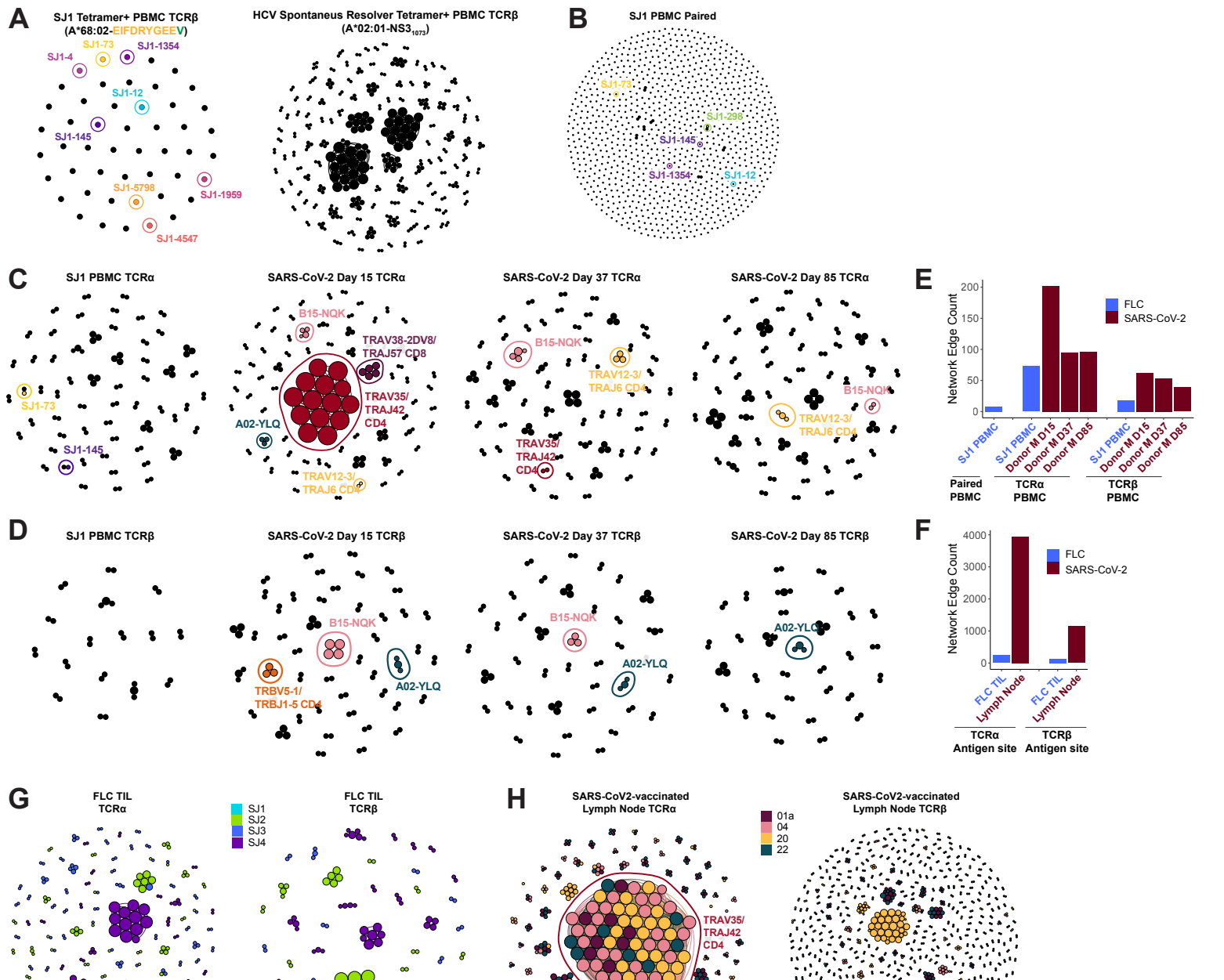


Figure S5. Comparison of TCRdist mapping for FLC TCR repertoires and viral-specific TCR repertoires, related to Figure 4. (A) Similarity network of TCR β chains from A*68:02-EIFDRYGEVV tetramer+ peripheral blood T cells from patient SJ1 (left, including clonotypes identified both pre- and post-antigen-specific expansion; see Figure S3D-G, Figure 3E,F) and A*02:01-NS3₁₀₇₃ tetramer+ peripheral blood T cells from HCV-infected patient SR5 who spontaneously resolved the infection [S3] (right). Each node corresponds to an individual TCR clonotype, and two nodes are connected by an edge if they have identical VJ-segments and fewer than 2 mismatches in the CDR3 amino acid sequence. Node size corresponds to node degree (number of neighbors). In the FLC network, cloned TCRs present are highlighted. Only cluster sizes ≥ 2 are shown for the HCV network. (B) TCRdist network of 1000 most abundant paired TCR clonotypes from patient FLC-SJ1 PBMCs. Each node represents a unique TCR clonotype, and two nodes are connected by an edge if their TCRdist<100; node size corresponds to node degree. Locations of cloned TCRs that are present among the top 1000 clones are highlighted. (C) Similarity network of TCR α chains from 1000 most abundant clonotypes from SJ1 PBMCs (far left) and PBMCs from a SARS-CoV-2-infected donor ("Donor M") at 15, 37, and 85 days post-infection [S4]. Each node corresponds to an individual TCR clonotype, and two nodes are connected by an edge if they have identical VJ-segments and fewer than 2 mismatches in the CDR3 amino acid sequence. Node size corresponds to node degree. In the FLC network, cloned TCRs present among the top 1000 clones are highlighted. In SARS-CoV-2 networks, clones reported to be specific for SARS-CoV-2 [S4-S6] are highlighted. (D) Same as C for 1000 most abundant TCR β clones in PBMCs from FLC patient SJ1 and SARS-CoV-2-infected Donor M. Colors matched across TCR α and TCR β networks indicate paired TCR chains. (E) Number of edges per network for networks of top clones in FLC and SARS-CoV-2-exposed PBMCs (B, C, and D), indicating "connectedness" of each network (F) Same as E for FLC and SARS-CoV-2-exposed T cells from sites of antigen presentation (G and H). (G) Similarity network of TCR α and TCR β chains from tumor-infiltrating T cells (TILs) from patients SJ1-SJ4. Each node corresponds to an individual TCR clonotype (n=1875 TCR α chains, 1877 TCR β chains), and two nodes are connected by an edge if they have identical VJ-segments and less than 2 mismatches in the CDR3 amino acid sequence. Node size corresponds to the node degree, and nodes are colored by patient. Only cluster sizes ≥ 2 are shown. (H) Same as E for the 500 most abundant TCR α and TCR β chains obtained from lymph node follicular helper cells of four SARS-CoV-2-vaccinated donors [S6]. Only cluster sizes ≥ 3 are shown for TCR α , and only cluster sizes ≥ 2 are shown for TCR β . Nodes are colored by patient, and large SARS-CoV-2-specific TCR α cluster is highlighted.

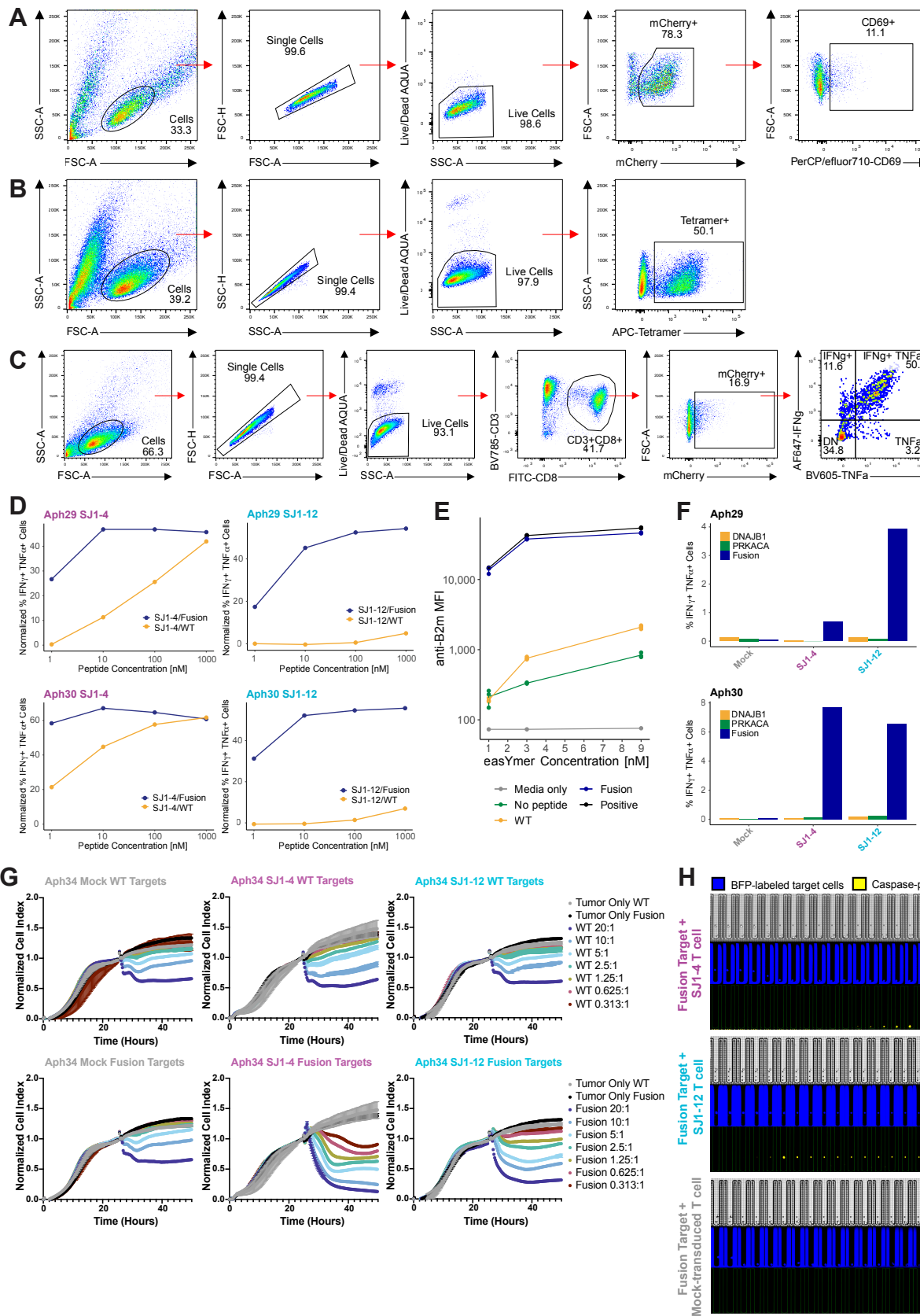


Figure S6: Additional data for validation of SJ1-4 and SJ1-12 specificity, function, and cytotoxicity in vitro, related to Figure 4 and 5. (A) Gating strategy for Figure 4B. (B) Gating strategy for Figure 4C and Figure 5A. (C) Gating strategy for Figure 5B-C and Figure S6D and F. (D) Same as Figure 5B, showing results for two additional donors. Normalized frequency of IFN γ +TNF α + cells among SJ1-4- or SJ1-12-transduced primary human T cells after stimulation with increasing doses of fusion (EIFDRYGE \bar{E} V) or WT peptide (EIFDRYGE \bar{E} EG) (see Methods for normalization formula). Data for SJ1-4 and SJ1-12 were collected in separate experiments. (E) Biochemical HLA binding assay results for fusion peptide EIFDRYGE \bar{E} V and WT peptide EIFDRYGE \bar{E} EG. The fusion peptide is classified as a strong binder, and the WT peptide is classified as a weak binder. (F) Same as Figure 5C, showing results for two additional donors. Frequency of IFN γ +TNF α + cells among SJ1-4 or SJ1-12 primary human T cells after stimulation with aAPCs expressing *DNAJB1-PRKACA* fusion or WT transgenes. All data were collected in the same experiment. (G) xCelligence assay measuring SJ1-4 or SJ1-12 transduced primary human T cell killing of fusion- or WT-expressing target cells, representing all E:T ratios tested. SJ1-12 and mock-transduced control data were collected in the same plate; SJ1-4 data were collected in a separate plate with an additional set of mock-transduced controls (comparable to those shown). (H) Select wells from Berkeley Lights Lightning assay co-culturing a single SJ1-4-, SJ1-12-, or mock-transduced primary human T cell with a single fusion-expressing aAPC for 24 hours. Images show brightfield (top), tagBFP-labeled targets (middle), and cleaved caspase-3 reporter of killing (bottom).

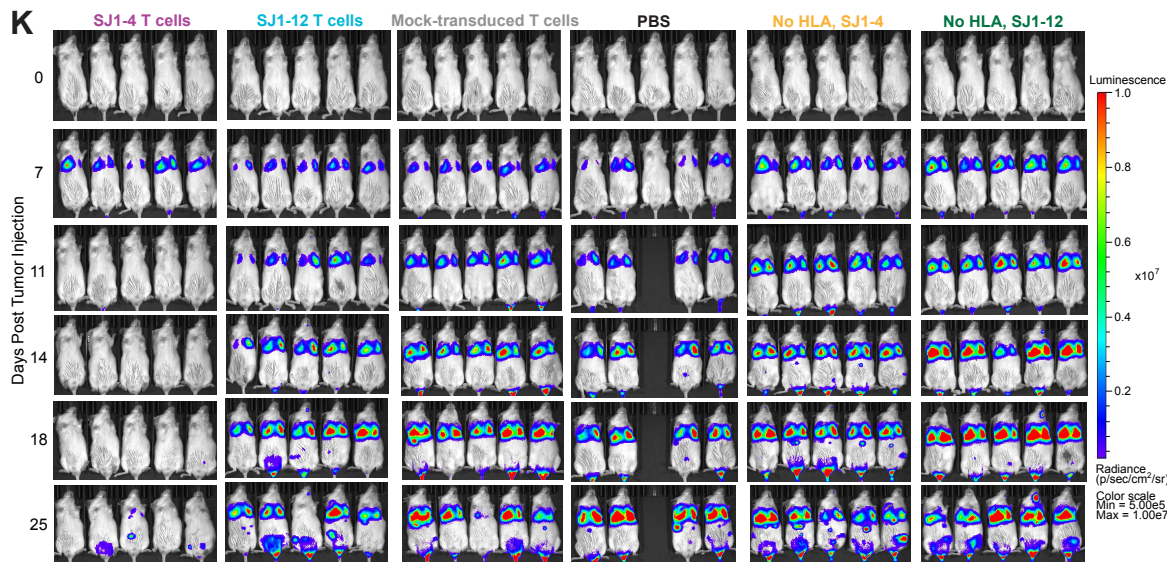
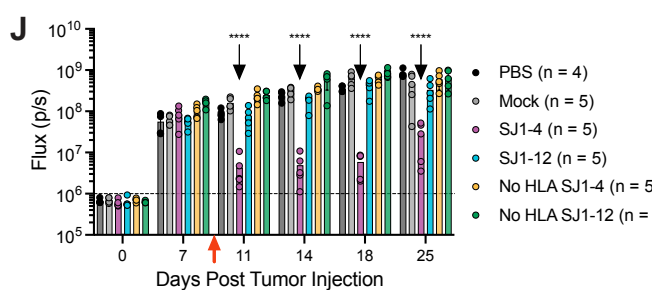
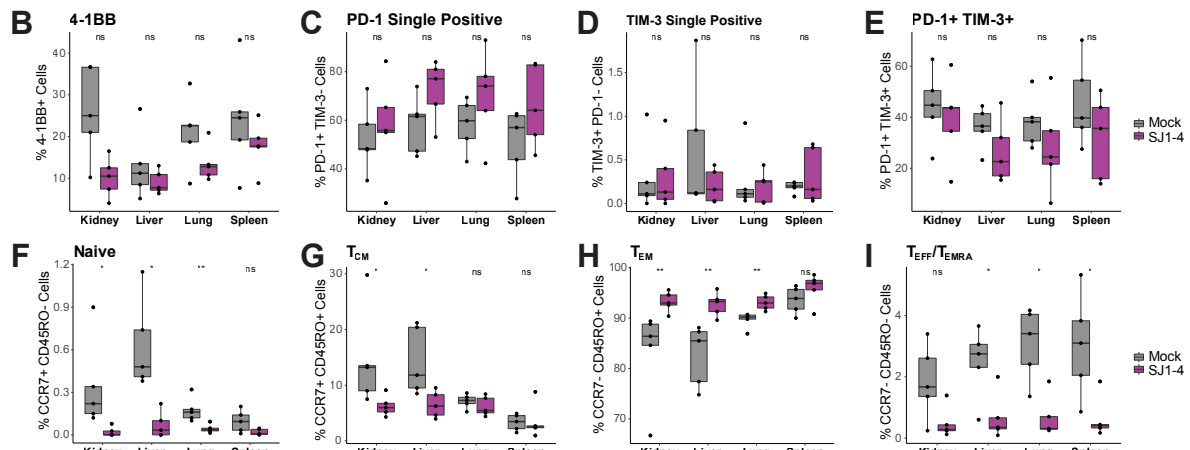
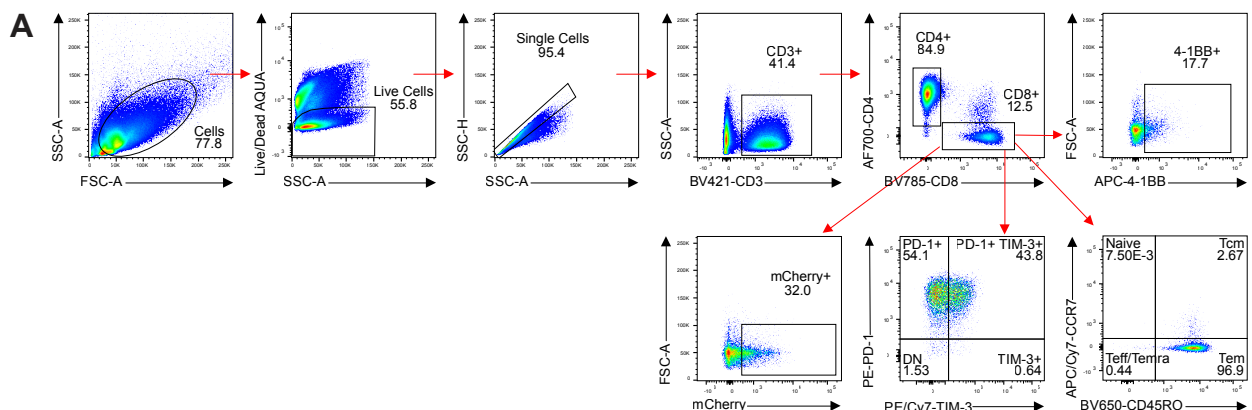


Figure S7. Additional data for in vivo activity of SJ1-4 and SJ1-12, related to Figure 6. (A) Gating strategy for Figure 6G and Figure S7B-I. (B-I) Frequency of 4-1BB+ (B), PD-1 single-positive (C), TIM-3 single-positive (D), PD-1+TIM-3+ (E), Naive CCR7+CD45RO- (F), T central memory (T_{CM}) CCR7+CD45RO+ (G), T effector memory (T_{EM}) CCR7-CD45RO+ (H), or T effector (T_{EFF})/T effector memory CD45RA+ (T_{EMRA}) CCR7-CD45RO- (I) CD8 T cells in kidneys, livers, lungs, and spleens harvested from mice treated with mock-transduced T cells or SJ1-4 T cells at euthanasia. Wilcoxon rank-sum test, * p < 0.05, ** p < 0.01, ns p > 0.05. (J) Tumor radiance measured by IVIS imaging for first 25 days of study, n=4-5 animals/group. Dashed line represents background bioluminescence (approximately 10⁶ p/s). Red arrow indicates day of T cell administration. 2-way ANOVA on log-transformed radiance values, *** p_{adj} < 0.0001. (K) IVIS images of tumor burden in mice treated with SJ1-4 T cells, SJ1-12 T cells, mock-transduced T cells, or PBS. Additional control mice received tumor lacking HLA-A*68:02 and were treated with either SJ1-4 T cells or SJ1-12 T cells.

Table S1: Bulk RNAseq patient cohort characteristics, related to Figure 1 and 2.

Patient ID	Sample Type	Sample Location	Age	Gender	Class I HLA Type	Number of Predicted Fusion Neoepitopes
FLC01	Metastatic	Unknown	24	F	A*02:01, A*01:01, B*08:01, B*07:05, C*07:01, C*15:05	2
FLC02	Metastatic	Extrahepatic	32	M	A*02:01, A*01:01, B*08:01, B*44:02, C*07:01, C*05:01	3
FLC03	Metastatic	Extrahepatic	19	M	A*02:01, A*03:01, B*51:01, B*15:01, C*03:03, C*01:02	0
FLC04	Metastatic	Extrahepatic	27	M	A*31:01, A*24:02, B*51:01, B*35:43, C*15:02, C*01:02	3
FLC05	Metastatic	Lymph node	25	F	A*23:01, A*01:01, B*51:01, B*44:03, C*04:01, C*15:02	7
FLC06	Recurrent	Liver	18	F	A*29:02, A*66:01, B*52:01, B*40:01, C*03:04, C*12:02	10
	Metastatic	Liver	20			
	Non-malignant liver	Liver	20			
	Metastatic	Peritoneal	20			
FLC07	Primary	Liver	16	M	A*02:01, A*32:01, B*14:01, B*44:02, C*05:01, C*08:02	3
FLC09	Primary	Liver	28	M	A*02:01, A*24:02, B*07:02, B*27:05, C*07:02, C*02:02	5
	Non-malignant liver	Liver	28			
FLC12	Recurrent	Liver	27	M	A*26:01, A*03:01, B*08:01, B*35:01, C*07:02, C*04:01	9
FLC13	Metastatic	Lung	17	F	A*01:01, A*03:01, B*08:01, B*07:02, C*07:02, C*07:01	4
	Metastatic	Lung	19			
FLC15	Metastatic	Ascites	48	F	A*02:01, A*02:01, B*57:01, B*15:01, C*06:02, C*03:03	0

FLC17	Metastatic	Lymph node	17	M	A*68:01, A*01:01, B*08:01, B*40:01, C*07:01, C*03:04	10
FLC18	Primary	Liver	15	F	A*02:01, A*01:01, B*44:03, B*44:02, C*05:01, C*16:01	5
	Metastatic	Lymph node	18			
	Metastatic	Unknown	18			
	Metastatic	Liver/Pancreas	18			
FLC20	Metastatic	Lymph node	19	M	A*02:01, A*03:01, B*27:05, B*07:02, C*02:02, C*07:02	3
FLC23	Primary	Liver	49	F	A*02:01, A*03:01, B*07:02, B*07:02, C*07:02, C*07:02	3
FLC25	Metastatic	Lymph node	22	F	A*32:01, A*26:01, B*44:02, B*27:14, C*01:02, C*05:01	7
	Metastatic	Lung	23			
FLC26	Primary	Liver	18	M	A*32:01, A*02:01, B*27:05, B*44:02, C*02:02, C*05:01	2
	Non-malignant liver	Liver	Unknown			
	Metastatic	Lymph node	18			
FLC27	Metastatic	Lymph node	18	F	A*03:01, A*23:01, B*44:03, B*55:01, C*03:03, C*04:01	7
	Non-malignant liver	Liver	18			
	Metastatic	Lymph node	18			
FLC29	Primary	Liver	Unknown			
	Metastatic	Lung	29	F	A*01:01, A*03:01, B*08:01, B*50:01 C*07:01, C*04:01	3
	Metastatic	Peritoneal	31	F	A*02:01, A*01:01, B*18:01, B*35:03, C*07:01, C*04:02	4
	Metastatic	Lymph node	27	F	A*23:01, A*01:01, B*51:01, B*44:03, C*04:01, C*15:02	7
FLC31	Metastatic	Lymph node	16	F	A*02:01, A*66:01, B*51:01, B*35:03, C*01:02, C*14:02	10

FLC33	Metastatic	Lung	54	M	A*11:01, A*03:01, B*35:01, B*14:02, C*04:01, C*08:02	6
FLC34	Non-malignant liver	Liver	18	M	A*24:02 A*25:01 B*44:02 B*18:01 C*05:01 C*12:03	11
	Primary	Liver	18			

Table S2: Fusion neoepitope predictions for patient and commercially available class I HLA alleles, related to Figure 1 and 2.

HLA	Peptide	Length	NetMHCcons1.1 Predicted IC ₅₀	NetMHCpan4.1b Predicted IC ₅₀	Fold Test Result
A*01:01	none				
A*02:01	none				
A*02:03	EIFDRYGEVV	10	359.95	813.84	Strong
	EVKEFLAKA	9	1854.1	977.8	Strong
	YGEEVKEFLAKA	12	18882.64	431.69	Strong
A*02:11	IFDRYGEVV	9	805.96	1413.12	N/A
	EIFDRYGEVV	10	50.51	964.05	N/A
	EIFDRYGEEVKEFL	14	365.84	15276.18	N/A
A*02:19	none				
A*03:01	none				
A*11:01	EVKEFLAK	8	446.91	13676.56	NB
	IFDRYGEEVKEFLAK	15	968.71	N/A	Weak
	EVKEFLAKAKEDFLK	15	390.37	N/A	Weak
A*23:01	RYGEEVKEF	9	126.7	66.82	N/A
	RYGEEVKEFL	10	592.1	603.45	N/A
	IFDRYGEEVKEF	12	846.17	2299.78	N/A
A*24:02	RYGEEVKEF	9	129.48	48.4	Strong
	RYGEEVKEFL	10	255.99	480.16	Weak
A*24:03	RYGEEVKEF	9	4.93	4.6	N/A
	RYGEEVKEFL	10	6.94	35.37	N/A
	RYGEEVKEFLA	11	973.97	2268.24	N/A
	IFDRYGEEVKEF	12	178.16	405.45	N/A
	RYGEEVKEFLAKA	13	864.68	9766	N/A
	REIFDRYGEEVKEF	14	3911.67	876.25	N/A
	FDRYGEEVKEF	11	13000.15	244.4	N/A
	DRYGEEVKEF	10	22209.93	384.07	N/A
A*24:07	RYGEEVKEF	9	270.42	217	N/A
	RYGEEVKEFL	10	418.12	560.29	N/A
A*25:01	EIFDRYGEEVKEF	13	163.39	4382.15	Weak
	EVKEFLAKAKEDF	13	898.05	4328.34	NB
A*26:01	EVKEFLAKA	9	685.22	443.48	Strong
	EIFDRYGEEVKEF	13	33.85	1394.62	Weak
	EVKEFLAKAKEDF	13	245.15	1756.44	Strong
	EIFDRYGEEVKEFL	14	398.91	12850.09	NB
	EVKEFLAKAKEDFL	14	731.18	10485.27	Weak
A*26:03	EVKEFLAK	8	482.07	9032.13	N/A
	EVKEFLAKA	9	805.96	339.55	N/A
	EIFDRYGEEVKEF	13	832.55	5307.93	N/A
	EIFDRYGEEVKEFL	14	953.12	11109.41	N/A
	EVKEFLAKAKEDFL	14	823.59	29816.58	N/A
	EVKEFLAKAK	10	1006.1	824.71	N/A
A*29:02	none				
A*30:01	EVKEFLAK	8	525.66	10517.54	N/A
	RYGEEVKEFLAK	12	551.89	2416.51	N/A
	RKREIFDRYGEEVK	14	685.22	9334.56	N/A
	RYGEEVKEFLAKA	13	5044.15	806.05	N/A
A*31:01	none				
A*32:01	none				

A*33:03	EVKEFLAK	8	300.06	3461.5	N/A
	EVKEFLAKAK	10	592.8	377.33	N/A
	EVKEFLAKAKEDFLK	15	150.95	N/A	N/A
A*66:01	EVKEFLAK	8	888.39	4723.51	N/A
	EVKEFLAKAK	10	1550.96	198.59	N/A
	EIFDRYGEVK	11	810.33	2380.33	N/A
	EIFDRYGEEVKEF	13	902.93	6862.59	N/A
	EVKEFLAKA	9	1477.25	429.11	N/A
A*68:01	EVKEFLAK	8	36.31	1046.48	Strong
	EVKEFLAKAK	10	82.19	30.43	Strong
	EIFDRYGEVK	11	18.37	148.81	Strong
	EVKEFLAKAKEDFLK	15	12.71	N/A	Strong
A*68:02	EVKEFLAKA	9	74.16	42.88	Strong
	EIFDRYGEV	10	11.05	23.59	Strong
	EIFDRYGEEVKEFL	14	10.52	1262.13	Weak
	EVKEFLAKAKEDFL	14	122	2670.59	Weak
	EIFDRYGEEVKEFLA	15	26.11	N/A	Strong
	EEVKEFLAKA	10	11233.42	551.7	Weak
B*07:02	DPRKREIFDRYGEV	15	989.9	N/A	NB
B*07:05	DPRKREIFDRYGEV	15	843.74	N/A	N/A
B*08:01	none				
B*14:01	none				
B*15:01	none				
B*15:03	FDRYGEVKEF	11	471.75	17085.96	N/A
	RKREIFDRYGEV	13	784.45	14125.49	N/A
	REIFDRYGEVKEF	14	73.76	3638.57	N/A
B*18:01	REIFDRYGEVKEF	14	270.22	8658.18	Weak
	EEVKEFLAKAKEDF	14	377.91	2976.71	Weak
B*27:05	none				
B*27:14	none				
B*35:01	EIFDRYGEVKEF	13	937.77	21437.63	NB
B*35:02	none				
B*35:03	none				
B*35:43	EIFDRYGEVKEF	13	362.98	16448.54	N/A
B*37:01	none				
B*38:01	none				
B*39:02	REIFDRYGEV	11	206.13	1277.79	N/A
	RKREIFDRYGEV	13	988.66	14674	N/A
	REIFDRYGEVKEFL	15	109.78	N/A	N/A
B*40:01	GEEVKEFL	8	45.09	1920.77	Strong
	REIFDRYGEV	11	34.59	442.81	Strong
	REIFDRYGEVKEF	14	139.66	6446.84	Strong
	REIFDRYGEVKEFL	15	8.52	N/A	Strong
	EEVKEFLAKAKEDFL	15	214.14	N/A	Strong
B*41:01	GEEVKEFLA	9	860.02	124.85	Strong
	REIFDRYGEV	11	227.27	371.82	Strong
	GEEVKEFLAKA	11	1290.38	712.88	Strong
	YGEEVKEFLA	10	24087.38	680.14	Strong
	EEVKEFLAKA	10	1103.02	592.38	Strong
	REIFDRYGEVKEFL	15	425.67	N/A	Strong
B*42:01	DPRKREIFDRYGEV	15	237.32	N/A	N/A
B*44:02	REIFDRYGEVKEF	14	312.72	1740.7	Weak
	EEVKEFLAKAKEDF	14	608.33	6776.26	NB

B*44:03	REIFDRYGEVKEF	14	153.95	2054.98	N/A
	EEVKEFLAKAKEDF	14	140.42	5080.14	N/A
	EEVKEFLAKAKEDFL	15	888.39	N/A	N/A
B*50:01	REIFDRYGEV	11	407.64	2810.45	N/A
B*51:01	none				
B*52:01	none				
B*55:01	none				
B*57:01	none				
C*01:02	none				
C*02:02	none				
C*03:02	YGEEVKEF	8	459.88	11733.83	N/A
	EIFDRYGEVKEF	13	562.55	24356.79	N/A
C*03:03	none				
C*03:04	none				
C*04:01	IDFRYGEV	9	8571.13	509.38	Strong
C*05:01	none				
C*06:02	none				
C*07:01	DRYGEVKEFL	11	797.29	18372.75	NB
C*07:02	RYGEEVKEF	9	534.26	775.03	Weak
	RYGEEVKEFL	10	995.27	7987.83	NB
C*08:02	IFDRYGEV	9	841.61	2393.5	N/A
C*12:02	none				
C*12:03	YGEEVKEFL	9	2936.57	10541.81	N/A
	EIFDRYGEV	10	283.7	13641.78	N/A
	EIFDRYGEVKEF	13	398.91	25634.37	N/A
	EIFDRYGEVKEFL	14	674.19	31186.59	N/A
C*14:02	IFDRYGEV	9	780.22	1027.49	N/A
	RYGEEVKEF	9	92.08	56.36	N/A
	RYGEEVKEFL	10	119.38	1827.41	N/A
	IFDRYGEVKEF	12	459.16	3909.05	N/A
	IFDRYGEVKEFL	13	459.16	11909.31	N/A
C*15:02	none				
C*16:01	none				

Table S3: Differentially expressed genes between SJ1-4-expressing cells and other cells in 10x dataset, related to Figure 3.

Gene	P value	Average Log ₂ (Fold Change)	Percent Expression in SJ1-4	Percent Expression in Other	P _{adj} value
TRBV15	1.19E-66	3.00539276	1	0.023	1.40E-62
TRAV6	1.29E-47	3.19205425	0.833	0.028	1.51E-43
TRAV16	2.93E-33	3.38520319	1	0.097	3.43E-29
GPR183	3.52E-18	1.5270049	0.5	0.036	4.12E-14
TBC1D4	8.03E-14	1.58606397	0.389	0.03	9.39E-10
CYP1B1	3.08E-13	1.53972423	0.333	0.021	3.61E-09
TNFRSF4	1.15E-11	1.3865279	0.444	0.051	1.35E-07
ZBED2	6.24E-11	2.28566369	0.556	0.093	7.30E-07
TNFRSF18	7.84E-09	1.88855054	0.722	0.197	9.17E-05
TNFRSF9	7.36E-08	2.65043616	0.333	0.047	0.00086169
MIR155HG	9.34E-07	1.41842231	0.333	0.055	0.01093398
TRBV7-3	1.22E-06	-3.9374121	0.167	0.716	0.01426843
GZMH	1.48E-06	1.92439497	0.611	0.193	0.01732025
GALNT2	2.21E-06	1.22605658	0.611	0.174	0.02584476
BACH2	3.49E-06	1.12759073	0.389	0.076	0.04081871
TRAV19	4.53E-06	-2.9966238	0.056	0.64	0.0529502
INPP5F	4.53E-06	1.06438533	0.333	0.057	0.05305553
TIGIT	6.67E-06	1.70364523	0.833	0.46	0.07809625
GZMB	1.31E-05	1.60665985	1	0.975	0.15353234
TRBC1	1.38E-05	-2.0392678	0.111	0.642	0.16093839
NELL2	1.96E-05	1.50487105	0.5	0.159	0.2290493
CTLA4	2.02E-05	2.38584296	0.5	0.155	0.23646321
IFNG	2.57E-05	3.06429968	0.5	0.163	0.3009463
TMSB4X	3.14E-05	-0.8692806	1	0.989	0.3675288
SNX6	3.93E-05	1.12929048	0.778	0.369	0.45989362
CSTF3	4.07E-05	0.8691818	0.278	0.051	0.47577759
ALG5	4.11E-05	1.01777295	0.444	0.121	0.48055126
SRSF9	4.19E-05	1.04332259	0.556	0.193	0.48978789
FTL	4.47E-05	-1.0605185	1	1	0.52338823
PAM	4.67E-05	1.52021039	0.333	0.076	0.54677162
MRPS22	5.02E-05	0.86137182	0.389	0.095	0.58735437
PKD2	5.13E-05	0.73935187	0.278	0.051	0.59987238
IL2RA	5.85E-05	1.88535111	0.778	0.481	0.68474686
ACSL4	7.06E-05	1.2507719	0.5	0.155	0.82588674
ZNF106	8.47E-05	0.97677804	0.611	0.227	0.99161962
ANKRD12	8.94E-05	0.94999744	1	0.667	1
EMC2	0.00012063	0.80310761	0.333	0.078	1
PIGT	0.00012519	0.84328687	0.5	0.159	1
CCL5	0.00014665	-1.1486503	1	0.975	1
RBPJ	0.00015677	1.33433031	0.778	0.443	1
RTL8A	0.00016631	0.81177644	0.333	0.078	1
IL32	0.00017153	-0.8233863	0.889	0.996	1
CD44	0.00017627	1.00540902	0.833	0.494	1
FXYD5	0.00017672	0.83506786	1	0.794	1
PACSin2	0.00020332	0.63766562	0.278	0.057	1
PTPRE	0.00021582	1.16242572	0.333	0.087	1
TRMT13	0.00022548	0.748784	0.333	0.081	1
HLA-DRB1	0.00022548	0.95202282	1	0.814	1
CERS5	0.00023477	0.81323264	0.333	0.083	1

RBMXL1	0.00024698	1.10430811	0.278	0.061	1
MAF	0.00027221	1.24327746	0.444	0.157	1
VEZT	0.00030334	0.84551205	0.389	0.114	1
ATP6V1A	0.00031831	0.7045777	0.278	0.061	1
PRPSAP2	0.00032306	0.86618217	0.278	0.061	1
IRF4	0.00042008	1.19068136	0.278	0.064	1
ARID5B	0.00042296	1.15853766	0.5	0.199	1
CEMIP2	0.00044068	1.22147366	0.389	0.123	1
PFN1	0.00045664	-0.7218403	1	0.966	1
HLA-DRB5	0.00046603	0.94615605	1	0.826	1
LGALS1	0.00052737	-1.5331116	0.444	0.771	1
KCNN4	0.0005331	0.8687958	0.444	0.148	1
SECISBP2L	0.00054216	1.4865735	0.556	0.25	1
S100A11	0.00070524	-1.2501804	0.5	0.818	1
OXCT1	0.00074511	0.92689233	0.389	0.127	1
CAPG	0.00079744	-1.645544	0.056	0.487	1
CCL4	0.00081437	2.68607443	0.778	0.646	1
AKAP10	0.00085419	0.69983808	0.333	0.091	1
EMP3	0.00101621	-1.2372784	0.389	0.771	1
FRMD4B	0.0010524	0.78628709	0.444	0.163	1
ARL4C	0.00107871	-0.8826164	0.5	0.814	1
AC017002.3	0.00122419	1.15739528	0.444	0.172	1
LAG3	0.00133935	1.01986378	0.833	0.614	1
RARRES3	0.00136862	-1.5168317	0.167	0.547	1
TEN1	0.00142695	0.63881583	0.278	0.072	1
RPS2	0.00146838	0.64140546	0.889	0.665	1
CD109	0.00152495	0.94263103	0.278	0.076	1
CD84	0.00171059	1.16642222	0.278	0.081	1
A1BG	0.00204192	0.83952152	0.333	0.106	1
HSP90AB1	0.00207941	1.06383702	0.889	0.693	1
FAAP20	0.00242614	0.78544374	0.389	0.136	1
ZBTB25	0.00242807	0.87651755	0.278	0.078	1
SPOCK2	0.00244421	0.82864547	0.722	0.394	1
LGALS3	0.00254874	0.96446413	0.833	0.532	1
RPS4X	0.00261137	-0.7877764	0.778	0.939	1
TIMP1	0.00272052	1.37597762	0.722	0.519	1
CTNNA1	0.00277014	1.32802476	0.333	0.114	1
ZMYM2	0.00292381	0.51623518	0.278	0.076	1
KANSL3	0.00295772	0.89737094	0.278	0.083	1
NT5C3A	0.00297426	0.96337181	0.444	0.189	1
CLSTN1	0.00326693	0.76305291	0.389	0.144	1
VRK2	0.00328885	0.54293287	0.278	0.081	1
LITAF	0.00330333	0.84624136	0.611	0.324	1
LINC01943	0.00339898	0.91536552	0.5	0.227	1
APLP2	0.00345958	0.95312404	0.333	0.114	1
CMTM6	0.00347821	1.08241532	0.778	0.511	1
STK17A	0.00374002	-1.4619766	0.056	0.396	1
HAUS1	0.00459457	0.78350832	0.333	0.112	1
MT-ND2	0.00466179	0.44925379	0.944	0.9	1
TMEM189	0.00498108	0.77767499	0.278	0.085	1
SASH3	0.00500165	-1.1879924	0.056	0.381	1
YEATS2	0.00507438	0.64315675	0.278	0.087	1
PLPP1	0.00542776	0.84279352	0.278	0.087	1

LIMD2	0.00547338	-0.8686449	0.5	0.767	1
CDK6	0.00547905	0.84553027	0.667	0.392	1
SAMSN1	0.00578409	0.67643463	0.778	0.619	1
SURF4	0.00598707	0.88630811	0.556	0.292	1
FAM32A	0.00633877	-1.2129215	0	0.305	1
ZFP36L1	0.00639371	1.25736125	0.722	0.513	1
CCDC141	0.00661821	0.85714916	0.278	0.089	1
CD52	0.00670346	-0.656564	0.889	0.966	1
SLC16A3	0.00681828	0.93670561	0.444	0.203	1
NPDC1	0.00701373	0.76640419	0.444	0.191	1
RBM48	0.00729022	0.59657724	0.278	0.091	1
LAYN	0.00736223	0.70503433	0.278	0.091	1
ST8SIA4	0.00764583	0.93814586	0.444	0.193	1
ARHGAP45	0.00765393	-1.1819649	0	0.294	1
HLA-B	0.00778796	0.29674755	1	1	1
MAST4	0.00783298	0.73670945	0.5	0.233	1
SRGN	0.00799848	0.57506467	0.944	0.936	1
HNRNPDL	0.00805417	0.58957774	0.722	0.409	1
LPAR5	0.00901921	0.71536524	0.278	0.093	1
RNF4	0.00909176	0.53860336	0.333	0.121	1
PSMD13	0.00915208	0.83195962	0.556	0.314	1
PPIL4	0.00965395	0.61074564	0.333	0.123	1
SH3BGRL3	0.00967156	-0.5662971	0.944	0.983	1
HOPX	0.00968558	-0.7713159	0.611	0.839	1
STAM	0.00972809	0.73783353	0.333	0.127	1
SPRY1	0.00985719	1.31574743	0.333	0.138	1
PIGBOS1	0.00998092	0.58834429	0.333	0.125	1
SLAMF1	0.00998235	0.90970891	0.611	0.362	1
EID1	0.00999247	0.92053429	0.722	0.544	1

Table S4: Sequences of TCRs selected for validation, related to Figure 4.

TCR ID	V β segment	CDR3 β	J β segment	V α segment	CDR3 α	J α segment
SJ1-4	TRBV15	CATSRVKTSGGYEQYF	TRBJ2-7	TRAV16	CALDMFSGGYNKLIF	TRAJ4
SJ1-12	TRBV5-4	CASSLGQTYEQYF	TRBJ2-7	TRAV12-2	CAVNVPGNQFYF	TRAJ49
SJ1-1	TRBV7-3	CASSFLGSTDTQYF	TRBJ2-3	TRAV19	CALSEAEDSGGSNYKLT	TRAJ53
SJ1-145	TRBV12-4	CASSLSVVGSYEQYF	TRBJ2-7	TRAV29/DV5	CAASDNTDKLIF	TRAJ34
SJ1-1354	TRBV27	CASSLSSGTAYEQYF	TRBJ2-7	TRAV13-1	CAASPIPGDYKLSF	TRAJ20
SJ1-1959	TRBV6-5	CASTRGGNTDTQYF	TRBJ2-3	TRAV13-1	CAASWEGSARQLTF	TRAJ22
SJ1-4547	TRBV15	CATSAGDSYQETQYF	TRBJ2-5	TRAV19	CALSEIQGGSEKLVF	TRAJ57
SJ1-5798	TRBV19	CASMGTGDAYGYTF	TRBJ1-2	TRAV16	CALSPYGGATNKLIF	TRAJ32
SJ1-73	TRBV6-5	CASSYQTSGHEQYF	TRBJ2-7	TRAV12-2	CAVKQNSGGYQKVTF	TRAJ13
SJ1-298	TRBV5-1	CASSLSAIYEQYF	TRBJ2-7	TRAV12-1	CVVNTGNQFYF	TRAJ49
SJ1-1460	TRBV5-4	CASSLGYEQYF	TRBJ2-7	TRAV12-1	CVVDTGNQFYF	TRAJ49
SJ1-4416	TRBV9	CASSPGQAYEQYF	TRBJ2-7	TRAV12-2	CAVIFNTGNQFYF	TRAJ49
SJ2-6	TRBV5-5	CASRSNSQARYGYTF	TRBJ1-2	TRAV38-2/DV8	CAYRSGGSNFGNEKLT	TRAJ48
SJ2-10	TRBV9	CASSAGQGPREGYTF	TRBJ1-2	TRAV23/DV6	CAARVGYSAGSYQLT	TRAJ28
SJ2-61	TRBV12-3	CASSLPAGFGNSPLHF	TRBJ1-6	TRAV9-2	CALRHSGNTPLVF	TRAJ29
SJ2-71	TRBV19	CASSVRGRDTEAFF	TRBJ1-1	TRAV20	CAVGVGSRLTF	TRAJ58
SJ2-126	TRBV19	CASSTSPQGGSYFKLGYTF	TRBJ1-2	TRAV29/DV5	CAAIDGSNYQLI	TRAJ33
SJ2-149	TRBV25-1	CASTARTSGRGADTQYF	TRBJ2-3	TRAV12-3	CAIREGGSEKLVF	TRAJ57
SJ3-1	TRBV4-3	CASSQDGAGQGYTF	TRBJ1-2	TRAV12-2	CASLGVGGGNKLTF	TRAJ10
SJ3-2	TRBV19	CASNPLGGNQPQHF	TRBJ1-5	TRAV35	CAAHTGTASKLTF	TRAJ44
SJ3-3	TRBV4-1	CASSQEVRMNTTEAFF	TRBJ1-1	TRAV8-4	CAVSDDYGGSQGNLIF	TRAJ42
SJ3-4	TRBV20-1	CSAKTTGEVPYEQYF	TRBJ2-7	TRAV1-1	CAVSRRPGGGNTPLVF	TRAJ29
SJ4-1	TRBV13	CASSPGQGSRTEAFF	TRBJ1-1	TRAV5	CAEGLLSGNTPLVF	TRAJ29
SJ4-2	TRBV4-1	CASSQEGGRLVTQYF	TRBJ2-3	TRAV12-2	CAVNILGNKL	TRAJ47
SJ4-73	TRBV27	CASSLSLGGRGPDQYF	TRBJ2-3	TRAV20	CAVIMDSNYQLI	TRAJ33

Table S5: Primer sequences for single-cell TCR sequencing by nested multiplex PCR, related to STAR Methods

Primer Type	Primer Name	Primer Sequence (5'-3') ^a
Forward External	hTRAV1-ext	AACTGCACGTACCAGACATC
	hTRAV2-ext	GATGTGCACCAAGACTCC
	hTRAV3-ext	AAGATCAGGTCAACGTTGC
	hTRAV4-ext	CTCCATGGACTCATATGAAGG
	hTRAV5-ext	CTTTCTGAGTGTCCGAG
	hTRAV6-ext	CACCTGACCTGCAACTATAC
	hTRAV7-ext	GCAAAATACAGGGATGGG
	hTRAV8-1-ext	CTCACTGGAGTTGGGATG
	hTRAV8-3-ext	CACTGTCTCTGAAGGAGCC
	hTRAV8-2,4-ext	GCCACCTGGTTAAAGG
	hTRAV8-6-ext	GAGCTGAGGTGCAACTACTC
	hTRAV8-7-ext2	CTAACAGAGGCCACCCAG
	hTRAV9-1_2-ext	TGGTATGTCCAATATCTGG
	hTRAV10-ext	CAAGTGGAGCAGAGTCCTC
	hTRAV12-1_3-ext	CARTGTTCCAGAGGGAGC
	hTRAV13-1-ext	CATCCTCAACCCTGAGTG
	hTRAV13-2-ext	CAGCGCCTCAGACTACTTC
	hTRAV14-ext	AAGATAACTCAAACCAACCAG
	hTRAV16-ext	AGTGGAGCTGAAGTGCAC
	hTRAV17-ext	GGAGAAGAGGATCCTCAGG
	hTRAV18-ext3	TCCAGTATCTAAACAAGAGCC
	hTRAV19-ext	AGGTAACTCAAGCGCAGAC
	hTRAV20-ext	CACAGTCAGCGGTTAAGAG
	hTRAV21-ext	TTCCCTGCAGCTCTGAGTG
	hTRAV22-ext	GTCCTCCAGACCTGATTCTC
	hTRAV23-ext	TGCTTATGAGAACACTGCG
	hTRAV24-ext	CTCAGTCACTGCATGTTCA
	hTRAV25-ext	GGACTTCACCACGTACTGC
	hTRAV26-1-ext	GCAAACCTGCCTTGAATC
	hTRAV26-2-ext	AGCCAATTCAATGGAGAG
	hTRAV27-ext	TCAGTTCTAAGCATCCAAGAG
	hTRAV29-ext	GCAAGTTAACAAAATTCA
	hTRAV30-ext	CAACAACCAGTGCAGAGTC
	hTRAV34-ext	AGAACTGGAGCAGAGTCCTC
	hTRAV35-ext	GGTCAACAGCTGAATCAGAG
	hTRAV36-ext	GAAGACAAGGTGGTACAAAGC
	hTRAV38-ext	GCACATATGACACCAGTGAG
	hTRAV39-ext	CTGTTCTGAGCATGCAG
	hTRAV40-ext	GCATCTGTGACTATGAAC
	hTRAV41-ext	AATGAAGTGGAGCAGAGTC
	hTRBV2-ext	TCGATGATCAATTCTCAGTTG
	hTRBV3-ext	CAAAATACCTGGTCACACAG
	hTRBV4-ext	TCGTTCTCACCTGAATG
	hTRBV5-1_4-ext	GATTCTCAGGKCKCCAGTTC
	hTRBV5-5_8-ext	GTACCAACAGGYCCTGGGT
	hTRBV6-1_3,5_9-ext	ACTCAGACCCCCAAAATTCC
	hTRBV6-4-ext	ACTGGCAAAGGAGAAGTCC
	hTRBV7-1_3-ext	TRTGATCCAATTCTCAGGTCA
	hTRBV7-4_9-ext new	CGSWTCTYTGCAGARAGGC
	hTRBV9-ext	GATCACAGCAACTGGACAG
	hTRBV10-1-ext	CAGAGCCCAGACACAAG
	hTRBV10-2-ext	ACCTTGATGTGTCACCAGAC
	hTRBV10-3-ext	CAGAGCCCAGACACAAG

	hTRBV11-ext hTRBV12-ext hTRBV13-ext hTRBV14-ext hTRBV15-ext hTRBV16-ext hTRBV17-ext hTRBV18-ext hTRBV19-ext hTRBV20-ext hTRBV23-ext hTRBV24-ext hTRBV25-ext hTRBV27,28-ext hTRBV29-ext hTRBV30-ext	CGATTTCAGAGACGC ARGTGACAGARATGGGACAA AGCGATAAAGGAAGCATCC CCAACAATCGATTCTAGCTG AGTGACCCTGAGTTGTTCTC GTCTTGATGAAACAGGTATGC CAGACCCCCAGACACAAG CATAGATGAGTCAGGAATGCC AGTTGTGAAACAGAATTGAACC AAGTTTCTCATCAACCATGC GCGATTCTCATCTCAATGC CCTACGGTTGATCTATTACTCC ACTACACCTCATCCACTATTCC TGGTATCGACAAGACCCAG TTCTGGTACCGTCAGCAAC TCCAGCTGCTCTTCACTCC
Reverse External	hTRAC-ext hTRBC-ext	GACCAGCTGGACATCACAG TAGAACTGGACTTGACAGCG
Forward Internal	hTRAV1-int hTRAV2-int hTRAV3-int hTRAV4-int hTRAV5-int hTRAV6-int hTRAV7-int hTRAV8-1-int hTRAV8-2,8-4-int hTRAV8-3-int hTRAV8-6-int hTRAV8-7-int hTRAV9-1,9-2-int hTRAV10-int hTRAV12-1,12-2,12-3-int hTRAV13-1-int hTRAV13-2-int hTRAV14-int hTRAV16-int hTRAV17-int hTRAV18-int hTRAV19-int hTRAV20-int hTRAV21-int hTRAV22-int hTRAV23-int hTRAV24-int hTRAV25-int hTRAV26-1-int hTRAV26-2-int hTRAV27-int hTRAV29-int hTRAV30-int hTRAV34-int hTRAV35-int hTRAV36-int	GCACCCACATTCTKCTTAC CACTCTGTGTCATGCTTAC ATGCACCTATTCACTCTGG ATTATATCACGTGGTACCAACAG TACACAGACAGCTCCTCCAC TGGTACCGACAAGATCCAG TATGAGAACAGAGAAAGGAAGAC GTCAACACCTTCAGCTCTC TTTGAGGCTGAATTAAAGAGG AGAGTGAACACCTCCTCCAC AACCAAGGACTCCAGCTTC ATCAGAGGTTTGAGGCTG GAAACCACCTCTTCCACTTG GAAAGAACTGCACTCTCAATG AAGATGGAAGGTTACAGCAC TCAGACAGTGCCTCAAACATAC CAGTGAAACATCTCTCTGC AGGCTGTGACTCTGGACTG GTCCAGTACTCCAGACAACG CCACCATGAACACTGCAGTTAC TGACAGTCCCTCCACCTG TGTGACCTGGACTGTGTG TCTGGTATAGGCAAGATCCTG AACTTGGTTCTCAACTGCAG CTGACTCTGTGAACAAATTGC TGCATTATTGATAGCCATACG TGCCTTACACTGGTACAGATG TATAAGCAAAGGCCTGGTG CGACAGATTCACTCCCAG TTCACCTGCCTTGTAAACCAC CTCACTGTGTACTGCAACTCC CTGCTGAAGGTCTACATTG AGAACATGGTGAAGCAC ATCTCACCATAAACTGCACG ACCTGGCTATGGTACAAGC ATCTCTGGTTGTCCACGAG

hTRAV38-int	CAGCAGGCAGATGATTCTC
hTRAV39-int	TCAACCACTTCAGACAGACTG
hTRAV40-int	GGAGGCAGAAATATTAAAGAC
hTRAV41-int	TTGTTTATGCTGAGCTCAGG
hTRBV2-int	TTCACTCTGAAGATCCGGTC
hTRBV3-int	AATCTTCACATCAATTCCCTG
hTRBV4-int	CCTGCAGCCAGAAGACTC
hTRBV5-1,5-2,5-3,5-4-int	CTTGGAGCTGGRSGACTC
hTRBV5-5,5-6,5-7,5-8-int	TCTGAGCTGAATGTGAACG
hTRBV6-1,6-2,6-3,6-5,6-6,6-7,6-8,6-9-int	GTGTRCCCAGGATATGAACC
hTRBV6-4-int	TGGTTATAGTGTCTCCAGAGC
hTRBV7-1,7-2,7-3-int	TCYACTCTGAMGWTCCAGCG
hTRBV7-4,7-5,7-6,7-7,7-8,7-9-int	TGRMGATYCAGCGCACA
hTRBV9-int	GTACCAACAGAGCCTGGAC
hTRBV10-1-int	TGGTATCGACAAGACCTGG
hTRBV10-2-int	TGGTATCGACAAGACCTGG
hTRBV10-3-int	GGAACACCAGTGACTCTGAG
hTRBV11-int	GACTCCACTCTCAAGATCCA
hTRBV12-int	CYACTCTGARGATCCAGCC
hTRBV13-int	CATTCTGAACTGAACATGAGC
hTRBV14-int	ATTCTACTCTGAAGGTGCAGC
hTRBV15-int	ATAACTTCCAATCCAGGAGG
hTRBV16-int	CTGTAGCCTTGAGATCCAGG
hTRBV17-int	TGTTCACTGGTACCGACAG
hTRBV18-int	CGATTCTGCTGAATTCC
hTRBV19-int	TTCCCTCTCACTGTGACATCG
hTRBV20-int	ACTCTGACAGTGACCAAGTGC
hTRBV23-int	GCAATCCTGTCCTCAGAAC
hTRBV24-int	GATGGATACAGTGTCTCTGA
hTRBV25-int	CAGAGAAGGGAGATCTTCC
hTRBV27,28-int	TTCYCCCTGATYCTGGAGTC
hTRBV29-int	TCTGACTGTGAGCAACATGAG
hTRBV30-int	AGAATCTCTCAGCCTCCAGAC

Reverse internal index^b	Hum_Acj TRAC INDEX	CGACTCAAGTGTGTGGNNNNNN
	Hum_Bcj TRBC INDEX	<u>GGGTCAAGGGTTCTGGATAT</u> <u>CGACTCAGATTGGTACNNNNNN</u> <u>ACACSTTKTCAGGTCCCTC</u>

^a Primers targeting human TRAV (TCR variable α) and TRBV (TCR variable β) are sense; primers targeting human TRAC (TCR constant α) and human TRBC (TCR constant β) are antisense.

^b Well-specific barcode sequence is in bold; C-segment-specific sequence is underlined.

SUPPLEMENTAL REFERENCES

- S1. Karosiene, E., Lundsgaard, C., Lund, O., and Nielsen, M. (2012). NetMHCcons: a consensus method for the major histocompatibility complex class I predictions. *Immunogenetics* *64*, 177–186. 10.1007/s00251-011-0579-8.
- S2. Reynisson, B., Alvarez, B., Paul, S., Peters, B., and Nielsen, M. (2020). NetMHCpan-4.1 and NetMHCIIPan-4.0: improved predictions of MHC antigen presentation by concurrent motif deconvolution and integration of MS MHC eluted ligand data. *Nucleic Acids Res.* *48*, W449–W454. 10.1093/nar/gkaa379.
- S3. Mazouz, S., Boisvert, M., Abdel-Hakeem, M.S., Khedr, O., Bruneau, J., and Shoukry, N.H. (2021). Expansion of Unique Hepatitis C Virus-Specific Public CD8+ T Cell Clonotypes during Acute Infection and Reinfection. *J. Immunol. Baltim. Md 1950* *207*, 1180–1193. 10.4049/jimmunol.2001386.
- S4. Minervina, A.A., Komech, E.A., Titov, A., Bensouda Koraichi, M., Rosati, E., Mamedov, I.Z., Franke, A., Efimov, G.A., Chudakov, D.M., Mora, T., et al. (2021). Longitudinal high-throughput TCR repertoire profiling reveals the dynamics of T-cell memory formation after mild COVID-19 infection. *eLife* *10*, e63502. 10.7554/eLife.63502.
- S5. Minervina, A.A., Pogorelyy, M.V., Kirk, A.M., Crawford, J.C., Allen, E.K., Chou, C.-H., Mettelman, R.C., Allison, K.J., Lin, C.-Y., Brice, D.C., et al. (2022). SARS-CoV-2 antigen exposure history shapes phenotypes and specificity of memory CD8+ T cells. *Nat. Immunol.* *23*, 781–790. 10.1038/s41590-022-01184-4.
- S6. Mudd, P.A., Minervina, A.A., Pogorelyy, M.V., Turner, J.S., Kim, W., Kalaidina, E., Petersen, J., Schmitz, A.J., Lei, T., Haile, A., et al. (2022). SARS-CoV-2 mRNA vaccination elicits a robust and persistent T follicular helper cell response in humans. *Cell* *185*, 603–613.e15. 10.1016/j.cell.2021.12.026.